Interference profiles with multiple spherical waves: general case

L. M. Zerbino, R. Torroba, N. Rodríguez, and M. Garavaglia

Centro de Investigaciones Opticas (CONICET-UNLP-CIC), Casilla de Correo 124, 1900 La Plata, Argentina

Received June 28, 1983; accepted January 10, 1984

Characteristics of multiple-beam interference fringes, as in a Fabry–Perot interferometer with monochromatic light, are analyzed. The optical path and the optical-path difference between interfering beams are calculated for the most general case. Different refractive indices in the inner and outer media, and arbitrary locations of the light source and the point of observation, are taken into account. An expression for the impulse response of the system is given. The results obtained from experimental tests confirm the theoretical predictions.

1. INTRODUCTION

As is well known, the analysis of the interferential processes in different optical structures must include a solution of the geometrical aspect that relates the fringe localization in the interferential pattern with the intensity distribution across it.

In the case of multiple-reflection interferometers, such as the Fabry–Perot interferometer, several kinds of experimental setups were employed. Plane-parallel or spherical mirrors were used in different kinds of scientific or metrological applications.[1–3]

The geometry and the intensity profile of the interference pattern produced by such optical structures are well known for the cases in which mirrors are at normal alignment conditions.

Recently, Brossel[4] and Aebischer[5] researched the geometry and the intensity profile of the interference pattern produced by a misaligned Fabry–Perot interferometer, and Rogers[6] developed a program to compute the profile of multiple-beam Fizeau fringes.

Our paper follows the methodology of Refs. 4–6 but introduces the more general conditions for the calculation of the optical-path difference, the impulse response, and the intensity-profile distribution, as shown in Section 2.

These general conditions are as follows: (1) Three different refractive indices in the entire optical structure are considered. (2) The light source can be placed near the interferometer, which implies the treatment of spherical waves. (3) The observation plane can also be placed near the interferometer. These conditions correspond to the generalization of the two-index case studies by Zerbino[7] and justify the design of a compact device for interferometric holography.[8]

In Section 3 the theoretical results obtained in Section 2 [Eq. (15)] are tested in those limiting cases previously reported, ensuring the consistency of the methodology employed and of the results.

Section 4 describes the experimental test of the theoretical results.

2. CALCULATION OF THE OPTICAL-PATH DIFFERENCE, THE IMPULSE RESPONSE, AND THE INTENSITY-PROFILE DISTRIBUTION

We analyze the optical-path difference as well as the impulse response and the intensity distribution of light in the interferential pattern produced by the most general case of a misaligned Fabry–Perot interferometer.

Optical-Path Difference

To calculate the optical-path difference between rays passing through a misaligned Fabry–Perot interferometer it is necessary to characterize the optical structure under consideration.

We consider a wedge with plane partial reflecting surfaces S_1 and S_2 forming an angle α. Figure 1 shows a cross section

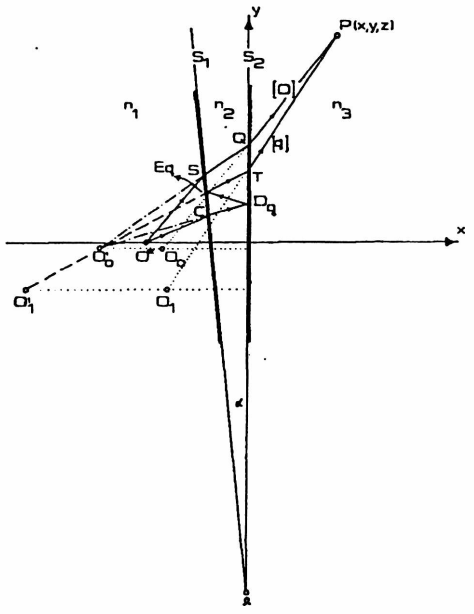

Fig. 1. Cross section of the wedge, showing the O^* real point source and its virtual images.

0740-3232/84/050495-07$02.00

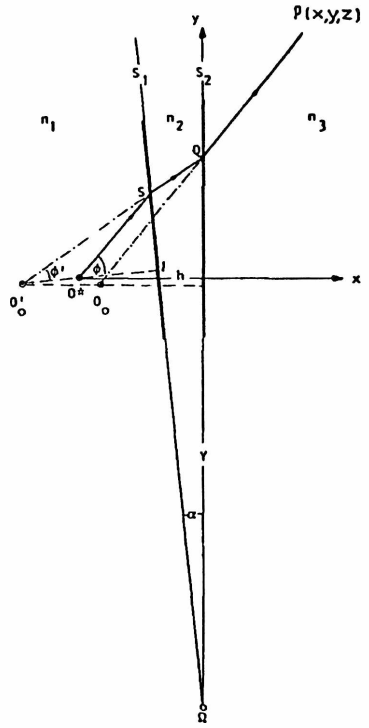

Fig. 2. Schematic diagram of the dihedral angle for the calculation of the positions of the virtual sources.

of the dihedral angle between S_1 and S_2, where Ω is the vertex of α, O^* is a light point source, and n_1, n_2, and n_3 are the refractive indices of the media. We take into account the multiple reflections of rays in the medium characterized by n_2 placed between S_1 and S_2.

There are rays (such as O) that arise from O^* and travel through the wedge without suffering reflections, and there are others (such as q) that are reflected q times on each surface before leaving the cavity.

We determine the difference between the optical-path lengths of rays such as $[q]$ and $[O]$ when both arrive at the same observation point P(x, y, z), interfering with each other. The optical path $\mathbf{r}_q$ for the $[q]$ ray is

$$\mathbf{r}_q = n_1\overline{O^*C} + n_2(\overline{CD_1} + \overline{D_1E_1} + \overline{E_1D_2} + \overline{D_2E_2} + \ldots + \overline{D_qE_q} + \overline{E_qT}) + n_3\overline{TP}; \quad (1)$$

for the $[O]$ ray it is

$$\mathbf{r}_0 = n_1\overline{O^*S} + n_2\overline{SQ} + n_3\overline{QP}. \quad (2)$$

Let O'_0 be the image of the source O^* that is due to the refraction at S_1, and let O'_i be the successive image positions of O'_0, O'_1, ..., O'_{i-1} generated by multiple reflections at the surfaces. Also, let O_i be the image of O'_i given by the refraction at S_2. The images $O'_0, \ldots, O'_i$ of the source O^*, which can be interpreted as virtual sources in the medium of index n_2, lie on a circumference of radius l, whose center is Ω, and they are separated from one another by an angular distance 2α. This circumference is in the plane containing the normal to the surface S_1 and the point source O^*, and it is normal to the edge of the wedge (in Fig. 1, the x–y plane).[7]

On the other hand, as O'_1 is an image of O'_0, we can write

$$\overline{O'_0C} + \overline{CD_1} + \overline{D_1E_1} + \overline{E_1D_2} + \ldots + \overline{D_qE_q} + \overline{E_qT} = \overline{O'_1T}.$$

Besides, as is shown in Fig. 2, the segment $\overline{O^*I}$ is parallel to the normal to surface S_1, and we may write for any light ray leaving the source O^* at an angle ϕ

$$\overline{O^*S}\sin\phi = \overline{SI} = \overline{O'_0S}\sin\phi'. \quad (4)$$

Combining Eq. (4) with Snell's law, $n_1 \sin\phi = n_2 \sin\phi'$, produces the following result:

$$\overline{O^*S} = \frac{n_1}{n_2}\overline{O'_0S}. \quad (5)$$

Then, in general, we may write

$$\overline{O'_iQ} = \overline{O_iQ}\frac{n_2}{n_3}, \qquad i = 0, 1, 2.... \quad (6)$$

Going back to Fig. 1 and using Eq. (5) for point C (the intersection with surface S_1), Eq. (3) for a ray that is reflected q times inside the wedge, and Eq. (6) for point T (the intersection with the surface S_2), we find that the length of the optical path $[q]$ is given by

$$\mathbf{r}_q = \frac{n_1^2 - n_2^2}{n_2}\overline{O'_0C} + \frac{n_2^2 - n_3^2}{n_2}\overline{O'_qT} + n_3\overline{O_qP}, \quad (7)$$

and, in the same way, we obtain for the optical path $[O]$

$$\mathbf{r}_0 = \frac{n_1^2 - n_2^2}{n_2}\overline{O'_0S} + \frac{n_2^2 - n_3^2}{n_2}\overline{O'_0Q} + n_3\overline{O_0P}. \quad (8)$$

Let $O^* = (-\rho, 0, 0)$ and $O'_i = (-x'_i, -y'_i, 0)$ be the coordinates of the point light source and their images given by refraction and reflection, respectively, and $O_i = (-x_i, -y_i, 0)$ be the corresponding refraction images of $O'_i = (-x'_i, -y'_i, 0)$.

Then, from Fig. 1 and using Eq. (6), we obtain

$$\overline{O'_0Q} = \frac{n_2}{n_3}\frac{x_0}{x + x_0}\overline{O_0P}, \qquad \overline{O'_qT} = \frac{n_2}{n_3}\frac{x_q}{x + x_q}\overline{O_qP}. \quad (9)$$

Defining the coordinates $T = (x_T, y_T, z_T)$ and $Q = (x_Q, y_Q, z_Q)$, we find it possible to calculate[7]

$$\overline{O'_0C} = \frac{n_2}{n_1}\frac{(\rho - h)\cos\alpha}{x'_q\cos[(2q+1)\alpha] + [z_T^2 + (y_T - y'_q)^2]^{1/2}\sin[(2q+1)\alpha]}\overline{O'_qT},$$

$$\overline{O'_0S} = \frac{n_2}{n_1}\frac{(\rho - h)\cos\alpha}{x'_0\cos\alpha + [z_Q^2 + (y_Q - y'_0)^2]^{1/2}\sin\alpha}\overline{O'_0Q}, \quad (10)$$

where h is the width of the wedge in the x–z plane ($y = 0$).

Points P, T, and Q are not necessarily in the x–y plane because the last expressions are valid for any angle at which light impinges upon the wedge.

Now, in order to calculate both optical paths $[q]$ and $[O]$ and their difference, we must know

(1) The coordinates of the image sources O'_i and O_i as functions of the wedge angle α and the position of O^*.

(2) The coordinates of points Q and T as functions of the positions of the observation point P(x, y, z) and O'_i.

Let h be the width of the wedge in the x–z plane and y be the distance between Ω and the origin of the coordinates, as illustrated in Fig. 2; then

$$h = y \tan \alpha.$$

As we already know that the coordinates of the source are $O^* = (=\rho, 0, 0)$, easy calculations give

$$\left.\begin{aligned} x_0' &= \rho + \left(\frac{n_2}{n_1} - 1\right)(\rho - h)\cos^2 \alpha \\ y_0' &= \left(\frac{n_2}{n_1} - 1\right)(\rho - h)\cos \alpha \sin \alpha \\ z_0' &= 0 \end{aligned}\right\} \text{ for } O_0' = (-x_0', -y_0', 0),$$

$$\left.\begin{aligned} x_q' &= x_0' \cos 2q\alpha + (y - y_0')\sin 2q\alpha \\ y_q' &= y - (y - y_0')\cos 2q\alpha + x_0' \sin 2q\alpha \\ z_q' &= 0 \end{aligned}\right\} \text{ for } O_q' = (-x_q', -y_q', 0),$$

$$\left.\begin{aligned} x_0 &= \frac{n_3}{n_2} x_0' \\ y_0 &= y_0' \\ z_0 &= 0 \end{aligned}\right\} \text{ for } O_0 = (-x_0, -y_0, 0),$$

$$\left.\begin{aligned} x_q &= \frac{n_3}{n_2} x_q' \\ y_q &= y_q' \\ z_q &= 0 \end{aligned}\right\} \text{ for } O_q = (-x_q, -y_q, 0). \tag{11}$$

Points T and Q are defined by the intersections between the y–z plane ($x = 0$) and the segments $\overline{O_qP}$ and $\overline{O_0P}$, respectively; such intersections give

$$\left.\begin{aligned} x_T &= 0 \\ y_T &= y\left(1 - \frac{x}{x + x_q}\right) - y_q\left(\frac{x}{x + x_q}\right) \\ z_T &= z\left(1 - \frac{x}{x + x_q}\right) \end{aligned}\right\} \text{ for } T = (x_T, y_T, z_T)$$

and

$$\left.\begin{aligned} x_Q &= 0 \\ y_Q &= y\left(1 - \frac{x}{x + x_0}\right) - y_0\left(\frac{x}{x + x_0}\right) \\ z_Q &= z\left(1 - \frac{x}{x + x_0}\right) \end{aligned}\right\} \text{ for } Q = (x_Q, y_Q, z_Q). \tag{12}$$

Combining Eqs. (11) and (12) and introducing the result into Eqs. (10) and using Eqs. (9), we can write Eqs. (7) and (8) as functions of $\overline{O_qP}$, obtaining the general expression that is valid for $q = 0, 1, \ldots, p$:

$$\mathbf{r}_q = \overline{O_qP}\left\{\frac{n_1^2 - n_2^2}{n_3} \frac{\frac{n_2}{n_1}(\rho - h)\cos \alpha}{\frac{n_2}{n_3}(x + x_q)\cos[(2q + 1)\alpha] + [z^2 + (y + y_q)^2]^{1/2} \sin[(2q + 1)\alpha]} + \frac{n_2^2 - n_3^2}{n_3} \frac{x_q}{x + x_q} + n_3\right\},$$

where

$$\overline{O_qP} = [(x + x_q)^2 + (y + y_q)^2 + z^2]^{1/2}. \tag{13}$$

Before using this last expression for searching the optical-path difference, we can make several approximations taking into account the different orders of magnitude that play a significant role and then subtract $\mathbf{r}_q$ from $\mathbf{r}_0$.

The order of magnitude of the main parameters involved is as follows:

The width h can measure several millimeters.

The angle α of the wedge is small. It is of the order of 10^{-4}–10^{-3} rad.

$y = h/\tan \alpha \approx h/\alpha \approx 100$ m.

q, the number of reflections, may be several times 10.

$2q\alpha \approx 2 \times 10 \times 10^{-3} \approx 0\ (10^{-2})$.

As we want to obtain a general formula for the optical path that is valid both when the source and the record are at infinity and when the source and the record are near the interferometer, we will consider the possibility that ρ ranges from 10^{-1} m to infinity. Then we can replace $\sin \alpha$ with α and $\cos \alpha$ with 1 and neglect h^2 compared with ρ^2 and also α^2 compared with 1; then Eq. (7) is reduced to

$$\mathbf{r}_q = \overline{O_qP}\left(\frac{n_1^2 - n_2^2}{n_3} \times \left\{\frac{\frac{n_2}{n_3}x_0 - h}{\frac{n_2}{n_3}(x + x_0) + 2qh + [z^2 + (y + y_0)^2]^{1/2}(2q + 1)\alpha}\right\} + \frac{n_2^2 - n_3^2}{n_3} \frac{x_0 + \frac{n_3}{n_2}2qh}{x + x_0 + \frac{n_3}{n_2}2qh} + n_3\right) \tag{14}$$

and $\mathbf{r}_0$ is obtained by replacing q with zero.

After finding the difference between $\mathbf{r}_q$ and $\mathbf{r}_0$ and rearranging terms, we obtain the following expression for the optical path:

$$\delta_q = \frac{n_1^2 - n_3^2}{n_1} \times 2q \left\{ \rho h \frac{n_3}{n_2}\left(\frac{1}{A} - \frac{A}{(x+\rho)^2}\right) + \frac{\rho\alpha y\left[(\rho - 2h)\frac{n_2}{n_1} + h\right]}{(x+\rho)A} - \frac{\rho^2\alpha h y\left[(2q+2)\frac{n_3}{n_1} - \frac{n_3}{n_2} - \frac{n_2 n_3}{n_1^2}\right]}{(x+\rho)^2 A} \right\}$$

$$+ \frac{n_2^2 - n_3^2}{n_2} \times 2q \left\{ \frac{h\alpha y\rho\left[(2q+2)\frac{n_2}{n_1} - 1\right]}{(x+\rho)A} + \frac{hA}{(x+\rho)} \right\}$$

$$- \frac{n_1^2 - n_2^2}{n_2}\frac{n_3^2}{n_1^2} \times 2q \left\{ \frac{(y^2+z^2)^{1/2}\alpha h\rho\left[(2q+2)\frac{n_1}{n_2} - 1\right]}{(x+\rho)A} + \frac{(\rho - h)(y^2+z^2)^{1/2}\alpha\frac{n_1}{n_3}A}{(x+\rho)^2} \right\}$$

$$+ \frac{n_3^2}{n_2} 2q \frac{(\rho + x)h}{A} + n_3 2q\alpha y \frac{\left[(\rho - h)\frac{n_2}{n_1} + h\right]}{A}, \quad (15)$$

where

$$A = [(x+\rho)^2 + Y^2 + Z^2]^{1/2}.$$

Equation (15) represents the optical-path difference between two rays arriving at the same observation point P, one directly transmitted through the wedge and the other transmitted after q reflections inside the wedge, when we make the approximations $h^2 \ll \rho^2$ and $\alpha^2 \ll 1$.

Impulse Response

In the preceding section we calculated the optical path $\mathbf{r}_q$ for light coming from source O^*, having q reflections inside the cavity and reaching observation point P.

The phase difference corresponding to each optical path $\mathbf{r}_q$ is $\phi_q = (2\pi/\lambda)\mathbf{r}_q$, where λ is the wavelength in free space.

Suppose that at plane π^* (see Fig. 3) there is a plane object that is illuminated by monochromatic light. Let $U(O^*)$ be the complex field amplitude of the object at plane π^*, and let $U(P)$ be the complex field amplitude at point π that contains observation point P.

Using the linearity property, we can express the complex amplitude U as function of U^*, that is,

$$U(P) = \iint_{-\infty}^{\infty} U(O^*)h(P, O^*),$$

where $h(P, O^*)$ is the amplitude at P coordinates in response to a point-source object at O^* and h is the impulse response of the optical system.

We calculate the complex amplitude of the field at point P in plane π (refractive index n_3) when the interferometer is illuminated by monochromatic light coming from a point source placed at $O^*(=\rho, 0, 0)$ in plane π^* (refractive index n_1).

As we have already said, the incident field amplitude U_i at point P_I of plane π_I of the system can be written as

$$U_i = A\frac{\exp(ik\mathbf{r}_{0I})}{r_{0I}},$$

where $\mathbf{r}_{0I}$ is the optical path from O^* to $P_I(0, \xi, \eta)$ without reflections inside the instrument and r_{0I} is the geometric distance from O^* (the image of O^* calculated at n_3) to P_I (see Fig. 4).

Let $K(\xi, \eta)$ be the pupil function at plane π_I. The field amplitude U_i' at the output of the system (and also at plane π_I) will be

$$U_i'(\xi, \eta) = AK(\xi, \eta)\sum_{q=0}^{p} t_1 t_2 (r_1 r_2)^q \frac{\exp(ik\mathbf{r}_{qI})}{r_{qI}},$$

where $\mathbf{r}_{qI}$ is $\mathbf{r}_q$ of Eq. (14) for point $P_I \equiv (0, \xi, \eta)$.

As a final step, if we use the Huygens–Fresnel principle, we find that the field amplitude at point P of π is

$$h(x, y, z, -\rho, 0, 0) = \frac{A}{i\lambda}\iint_{-\infty}^{\infty} K(\xi, \eta) \times \frac{\exp(ikn_3 r_I)}{r_I}\left[\sum_{q=0}^{p} t_1 t_2 (r_1 r_2)\frac{e^{ik\mathbf{r}_{qI}}}{r_{qI}}\right]\cos(\bar{n}, \bar{r}_I)\,d\xi\,d\eta,$$

where

$$r_I = [x^2 + (y - \xi)^2 + (z - \eta)^2]^{1/2},$$

$$r_{qI} = [x_q^2 + (y_q - \xi)^2 + (z_q - \eta)^2]^{1/2},$$

and $\mathbf{r}_{qI}$ is given from Eq. (14) for $x = 0, y = \xi$, and $z = \eta$.

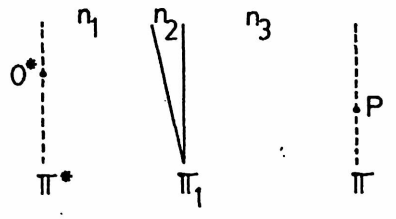

Fig. 3. Diagram showing the positions of the object and observation planes.

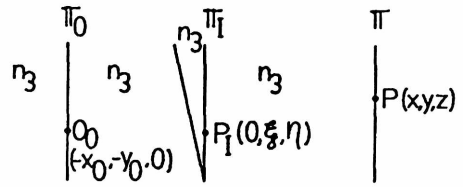

Fig. 4. Diagram of the relative positions of the object and observation planes referring to a medium of index n_3.

Intensity-Profile Distribution

In order to corroborate Eq. (15), we must calculate the transmitted amplitude and intensity through the wedge and the recorded intensity at point P.

Taking into account that observation point P is placed a finite distance from the wedge and supposing that the pupil is large, we can write the transmitted vibrations as

$$A_t = \sum_{q=0}^{p} t_1 t_2 (r_1 r_2)^q \frac{e^{ikr_q}}{r_q} A_i, \tag{16}$$

where $k = 2\pi/\lambda$, $\mathbf{r}_q$ is given by Eq. (14), and $r_q = [(x + x_q)^2 + (y + y_q)^2 + z^2]^{1/2}$, where the term e^{ikr_q}/r_q characterizes the spherical wave that reaches point P as coming from point O_q, with

$$\frac{r_0}{r_q} \simeq 1 - \frac{2\epsilon q \alpha}{r_0^2},$$

where

$$\left\{\left(\frac{n_3}{n_2}y\right)^2 + \left[\left(\frac{n_2}{n_1} - 1\right)(\rho - h) + \rho\right]^2\right\} 4q^2\alpha^2 \ll r_0^2$$

and

$$\epsilon = \frac{n_3}{n_2} y(x + x_0) + \left[\left(\frac{n_2}{n_1} - 1\right)(\rho - h) + \rho\right](y + y_0). \tag{17}$$

We can write Eq. (16) as

$$A_t = \left[1 + \sum_{q=1}^{p} (r_1 r_2)^q e^{ik\delta q}\left(1 - \frac{2\epsilon q\alpha}{r_0^2}\right)\right] t_1 t_2 A_i \frac{e^{ikr_0}}{r_0}, \tag{18}$$

where e^{ikr_0}/r_0 is the spherical wave coming from the real light source O^* and reaching point P.

The center of the spherical wave is at point $O_0(=x_0, =y_0, 0)$, and

$$r_0 = [(x + x_0)^2 + (y + y_0)^2 + z^2]^{1/2}.$$

Then the transmitted intensity for monochromatic light can be calculated as

$$I_t = A_t A_t^* = |A_t|^2. \tag{19}$$

With that intensity equation it is possible to plot the theoretical intensity profile for comparison with the experimental microdensitometric record of the interference pattern.

3. ANALYSIS OF LIMITING CASES

Equation (15) reproduces the theoretical expression of δ for the limiting cases already known:

(1) When $\alpha = 0$ and $n_1 = n_2 = n_3 = n$, the optical-path difference given by Eq. (15) take the form

$$\delta_q = 2qn \frac{(x + \rho)h}{[(x + \rho)^2 + y^2 + z^2]^{1/2}}. \tag{20}$$

If the observation point is placed at infinity, we obtain

$$\delta_q = 2qhn \cos\Theta \left\{1 + \frac{\rho(\cos\Theta)^{-1}}{[x^2 + y^2 + z^2]^{1/2}}\right\} \quad \text{for } x \gg \rho \tag{21}$$

and

$$\delta_q = 2qhn \cos\Theta \qquad \text{for } x \to \infty, \tag{22}$$

where

$$\cos\Theta = x/[x^2 + y^2 + z^2]^{1/2}.$$

These results correspond to the well-known concentric rings, whose theoretical intensity profile, calculated using Eqs. (18) and (19), is shown in Fig. 5(a).

(2) When $\alpha = 0$, $n_1 \neq n_2 = n'$, and $n_1 = n_3 = n$, the optical-path difference is

$$\delta_q = 2qh\left[\frac{n'(x + \rho)}{(x^2 + y^2 + z^2)^{1/2}} + \frac{(y^2 + z^2)(n'^2 - n^2)}{n'(x^2 + y^2 + z^2)^{1/2}}\right], \tag{23}$$

and, in the case when $x \gg \rho$ and $\rho/(x^2 + y^2 + z^2)^{1/2} \ll 1$, it results in

$$\delta_q = 2qh\left(n' \cos\Theta + \frac{n'^2 - n^2}{n'} \frac{\sin^2\Theta}{\cos\Theta}\right). \tag{24}$$

If the observation is made in a position near the axis ($\sin^2\Theta \ll 1$), the optical-path difference has the expression

$$\delta_q = 2qhn' \cos\Theta, \tag{25}$$

which also corresponds to concentric rings.

(3) When $\alpha \neq 0$ and $n_1 = n_2 = n_3 = n$, the optical-path difference is

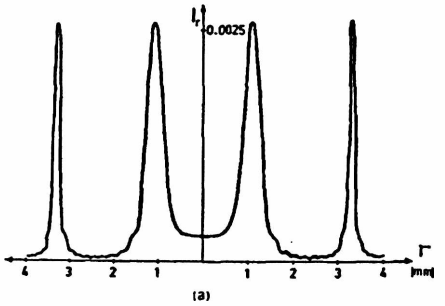

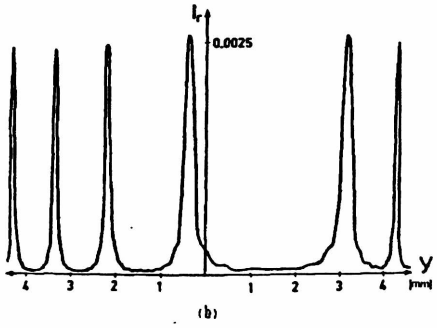

Fig. 5. Computed profiles for $\lambda = 632.8$ nm, $n = n' = 1$, $R = 0.8$, $h = 20$ mm, $\rho = 250$ mm, and $x = 300$ mm, where $r = (y^2 + z^2)^{1/2}$. For the calculations we used $p = 10$ and $I_r = I_t/I_i$: (a) $\alpha = 0$, (b) $\alpha = 2 \times 10^{-4}$ rad. The recording was taken for $z = 0 \Rightarrow r \equiv y$.

$$\delta_q = 2qhn\left[\frac{x+\rho}{(x^2+y^2+z^2)^{1/2}} + \frac{2q\alpha yn\rho}{(x^2+y^2+z^2)^{1/2}}\right], \quad (26)$$

and, for the case when $x \gg \rho$,

$$\delta_q = 2qn\left[h\cos\Theta + \frac{\alpha y\rho}{(x^2+y^2+z^2)^{1/2}}\right] \times\left[1 - \frac{\rho\cos\Theta}{(x^2+y^2+z^2)^{1/2}}\right]. \quad (27)$$

We can also neglect terms in $\rho\cos\Theta/(x^2+y^2+z^2)^{1/2}$, but, in the case of off-axis observation, we must retain the term $\alpha y\rho/(x^2+y^2+z^2)^{1/2}$, obtaining

$$\delta_q = 2qn\left[h\cos\Theta + \frac{\alpha y\rho}{(x^2+y^2+z^2)^{1/2}}\right], \quad (28)$$

which corresponds to interference patterns whose intensity profiles have symmetry only with respect to the z axis, as is shown in Fig. 5(b), which is the theoretical profile for $z = 0$.

We can add a comment for the case of close axis observation. If $y \approx 0$, Eq. (28) coincides with Eq. (22), which means that a small interferometer misalignment does not modify the structure of the central rings. This is also true if $y \approx z \approx 0$ and $n = n_1 = n_3 \neq n_2 = n'$ in Eq. (15). In this case, we again obtain Eq. (22).

4. EXPERIMENTAL RESULTS

The theoretical intensity profiles computed from Eq. (19) were plotted using an IBM/360 computer with a 2250 visual unity. Such plots were compared with the experimental microdensitometric records obtained for typical values of the parameters involved.

Figure 6 is a schematic of the experimental setup used. For the simulation of the light point source O^* we used a cw 1.5-mW He–Ne laser and a beam collimator. Those cases with $n_1 = n_3 \neq n_2$ were tested with a glass fixed interferometer of 7.6-mm width, and those cases with $n_1 = n_2 = n_3$, with an air-scanning Fabry–Perot interferometer. For recording the interference pattern we used Ilford PAN-F film (50 ASA).

The intensity densitometric profiles of the photographic records were scanned with a Grant automatic microdensitometer comparator.

We have observed an adequate coincidence between the theoretical and the experimental profiles. Figures 7(a) and 7(b) and 8(a) and 8(b) reproduce two examples of such coincidence.

The influence of changes in light-source position (ρ coordinate) and the observation plane (x coordinate) on the intensity distribution of interference patterns was also analyzed.

Figure 8(c) shows the experimental profile when $x = 300$ mm and $\rho = \infty$. Compare it with the trace in Fig. 8(b). Figure 8(d) shows the experimental profile when $x = 300$ mm and $\rho = 500$ mm. Compare it with the other experimental traces.

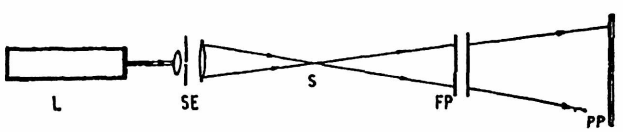

Fig. 6. Experimental setup: L, laser; SE, system of spatial-filter expansor beam collimator; S, light point source; FP, Fabry–Perot interferometer; PP, photographic plate.

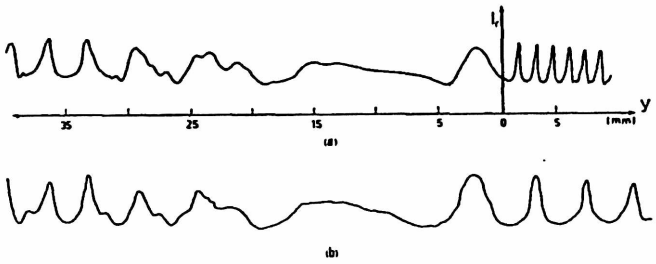

Fig. 7. (a) Theoretical and (b) experimental profiles showing the case $\lambda = 632.8$ nm, $n = 1$, $n'' = 1.5$, $h = 7.6$ mm, $R = 0.46$, $p = 10$, $\rho = 250$ mm, $x = 300$ mm, $\alpha = 2 \times 10^{-4}$ rad.; $z = 0 \Rightarrow r = y$. Discrepancies at the right-hand side are due to the mismatch between the microdensitometric record scanning direction and the meridional section of the interference pattern.

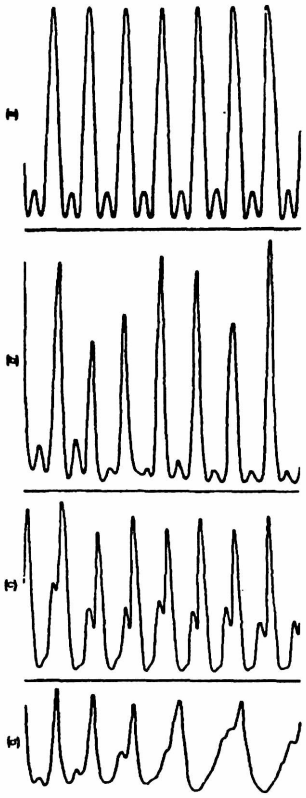

Fig. 8. Panel with different profiles corresponding to $\lambda = 632.8$ nm, $n = n'' = 1$, $h = 20$ mm, $R = 0.8$, $p = 10$, $\alpha = 2 \times 10^{-4}$ rad, $z = 0$: (a) and (b) theoretical and experimental profiles for $\rho = -\infty$ and $x = -500$ mm, respectively; (c) and (d) experimental profiles for $x = -300$ mm, with $\rho = -\infty$ and $\rho = 500$ mm, respectively.

ACKNOWLEDGMENTS

The invaluable support provided by the Subsecretaría de Ciencia y Tecnología, Argentina, is gratefully acknowledged.

REFERENCES

1. K. W. Meissner, "Interference spectroscopy." Part I, J. Opt. Soc. Am. 31, 405–427 (1941); Part II, J. Opt. Soc. Am. 32, 185–210 (1942).

2. J. E. Sears and H. Barrell, "Fundamental standards of length in terms of wave-lengths of light," Phil. Trans. R. Soc. London Ser. A **223**, 143–216 (1934).
3. P. Connes, "Increase of the product of luminosity and resolving power of interferometers by using a path difference independent of the angle of incidence," Rev. Opt. **35**, 37 (1956).
4. J. Brossel, "Multiple beam localized fringes." I. Intensity distribution and localizations; II. Conditions of observation and formations of ghosts," Proc. Phys. Soc. **59**, 224–242 (1947).
5. N. Aebischer, "Calculs de profils dissymétriques observables sur des figures d'interferences en ondes multiples sphériques," Nouv. Rev. Opt. Appl. **2**, 351–366 (1971).
6. J. Rogers, "Fringe shifts in multiple-beam Fizeau interferometry," J. Opt. Soc. Am. **72**, 638–643 (1982).
7. L. M. Zerbino, Doctoral Thesis (Universidad Nacional de La Plata, La Plata, Argentina, 1978).
8. L. Zerbino, H. Rabal, and M. Garavaglia, "Compact device for interferometric holography," Proc. Soc. Photo-Opt. Instrum. Eng. **210**, 188–195 (1979).